coatings

MDPI

Article

Icephobic Properties of Superhydrophobic Coatings Developed for Aeronautical Applications

Filomena Piscitelli [1,*], Matteo Fanciullo [2], Antonella Sarcinella [2], Mario Costantini [1] and Mariaenrica Frigione [2]

[1] Italian Aerospace Research Centre, CIRA, Via Maiorise, 1, 81043 Capua, Italy; m.costantini@cira.it
[2] Innovation Engineering Department, University of Salento, Prov. le Lecce-Monteroni, 73100 Lecce, Italy; matteo.fanciullo@studenti.unisalento.it (M.F.); antonella.sarcinella@unisalento.it (A.S.); mariaenrica.frigione@unisalento.it (M.F.)
* Correspondence: f.piscitelli@cira.it

Abstract: Ice accumulation poses a significant hazard to aviation safety, particularly in cold weather conditions, as it can compromise aerodynamic performance, increase structural weight, and diminish lift, occasionally resulting in severe stall incidents. At present, such risks are managed through the use of energy-demanding active ice protection systems (IPSs), which operate either by inhibiting ice formation (anti-icing) or by removing existing ice (de-icing). Nonetheless, in the context of future sustainable aviation, there is a pressing need to develop IPSs with lower energy requirements. A promising approach involves hybrid IPSs that integrate conventional active systems with passive superhydrophobic or icephobic surface treatments, which are capable of preventing, delaying, or minimizing ice buildup. These systems offer the potential to substantially decrease the energy consumption and consequently the CO_2 emissions. Furthermore, in accordance with FAA regulations, active IPSs are not permitted to operate during takeoff and initial flight stages to prevent any reduction in engine thrust. These two reasons emphasize the critical importance of developing efficient coatings that, on the one hand, promote the mobility of water droplets, hereby preventing ice formation, as achieved by superhydrophobic surfaces, and on the other hand, facilitate ice detachment, as required for icephobic performance. In this context, the primary objective of the present work is to emphasize the icephobic properties of two superhydrophobic coatings. To achieve this, an extensive characterization is first conducted, including wettability, Surface Free Energy (SFE), and surface roughness, to confirm their superhydrophobic nature. This is followed by an assessment of their icephobic performance, specifically in terms of ice adhesion strength, with comparisons made against a commercial aeronautical coating. The results revealed a significant reduction in both the wettability and SFE of the developed coatings compared to the reference, along with a marked decrease in ice adhesion strength, thereby demonstrating their icephobic properties. Future activities will focus on the combination of coatings with active IPS in order to assess the energy efficiency under extensive icing conditions where both superhydrophobic and icephobic properties are required.

Keywords: contact angle; ice adhesion test; icephobic coatings; superhydrophobic coatings; surface free energy; passive IPS; aeronautical coatings; energy efficient IPS

check for updates

Academic Editor: Eduardo Guzmán

Received: 31 March 2025
Revised: 12 May 2025
Accepted: 20 May 2025
Published: 22 May 2025

Citation: Piscitelli, F.; Fanciullo, M.; Sarcinella, A.; Costantini, M.; Frigione, M. Icephobic Properties of Superhydrophobic Coatings Developed for Aeronautical Applications. *Coatings* **2025**, *15*, 621. https://doi.org/10.3390/coatings15060621

Copyright: © 2025 by the authors. Licensee MDPI, Basel, Switzerland. This article is an open access article distributed under the terms and conditions of the Creative Commons Attribution (CC BY) license (https://creativecommons.org/licenses/by/4.0/).

1. Introduction

The formation of ice on aircraft surfaces during flight is a critical issue that can significantly affect flight safety and performance. Ice accumulation on wings, tail surfaces, and

other critical components disrupts the aerodynamics of the aircraft, leading to reduced lift, increased drag, and potential control difficulties. Additionally, ice formation on navigation or ice detection instruments during flight can disrupt their functionality, leading to inaccurate readings and compromised safety. It can affect airspeed, altitude, and ice detection, impair control surfaces, and reduce aircraft stability, increasing the risk of accidents [1].

In extreme cases, ice buildup can lead to mechanical failures or loss of control, emphasizing the importance of effective ice protection strategies [2–4]. Currently, the risks associated with ice accretion are mitigated through the use of energy-demanding active ice protection systems (IPSs). These systems function by either preventing the formation of ice (anti-icing) or removing ice once it has accumulated (de-icing). Anti-icing systems typically work by maintaining surface temperatures above freezing to prevent ice from forming in the first place, while de-icing systems focus on eliminating ice that has already accumulated by applying heat, chemicals, or mechanical forces [5,6]. While these active systems are effective in mitigating the dangers posed by ice, they come with significant energy consumption and maintenance challenges. Consequently, improving the efficiency and durability of these systems, particularly to reduce their energy demand and then the CO_2 emissions, remains a critical area of focus.

To address these challenges, there is a growing interest in developing passive coatings that can work synergistically with active IPSs with the primary goal of enhancing their energy efficiency [7,8]. These coatings, which are typically designed to reduce or prevent ice accumulation, minimize adhesion, or delay water freezing on their surface, offer significant potential to improve the overall energy efficiency of IPSs [9–16]. By reducing the initial ice accumulation or making it easier to remove, passive coatings could reduce the need for active systems to operate continuously, thus conserving energy and extending the life of active components [17]. However, the development of these coatings requires a thorough understanding of how they perform in real-world conditions and, among other things, how they can promote the mobility of water droplets and facilitate the ice detachment if used in combination with a de-icing active IPS. Therefore, both low wettability and low ice adhesion are essential. There are several techniques for testing ice adhesion on flat surfaces, which can generally be categorized into two main types: direct mechanical testing and centrifuge testing. In direct mechanical testing, the ice is detached from the material by applying a mechanical force, directly aiming to separate it from the surface being evaluated [18–21]. In centrifuge testing, centrifugal force is employed to remove the ice, relying on indirect forces [22–25]. However, ice adhesion tests conducted using different techniques produce varying results, e.g., Rønneberg et al. highlighted significant differences and variations across all configurations conducting tests in separate laboratories under similar conditions [26]. This underscores the necessity for a standardized method to enable consistent data comparison. In the absence of such a standardized approach, only comparative tests performed within the same laboratory, utilizing the same technology, can yield meaningful and reliable results.

In this context, the present study aims to demonstrate the icephobic properties of two superhydrophobic coatings by employing a simplified and accessible custom-built vertical shear test setup [26] for the evaluation of ice adhesion. The superhydrophobic nature of the coatings was confirmed through characterization of their wettability, Surface Free Energy (SFE), and surface roughness.

2. Materials and Methods

2.1. Materials

This study examines the hydrophobic and icephobic properties of two nanostructured multilayer coatings made of hydrophobic silica in epoxy resin [27,28]. Coatings were

applied with an airbrush at 3 bar pressure with dehumidified air. After the application, coatings were cured at 80 °C.

Composite specimens, consisting of carbon fibers and DGEBA epoxy resin, selected to simulate the structural components of an aircraft, were used as substrates. These specimens were gently abraded using SiC P 400 sandpaper and subsequently cleaned with Metaflex SP 1050, distilled water, isopropyl alcohol, and ethyl alcohol. Following this cleaning procedure, the commercial paint AkzoNobel Aerowave 5001 was applied using an airbrush at 3 bar pressure with dehumidified air. The AkzoNobel paint served as reference and as base layer for the application of developed coatings, which were then directly applied onto it without any further pre-treatment.

Composite specimens coated only with AkzoNobel paint are labeled as "REF", while those treated with the two superhydrophobic coatings are identified as "C-1" and "C-2", respectively. As shown in Figure 1, these coatings are visually indistinguishable from the reference layer.

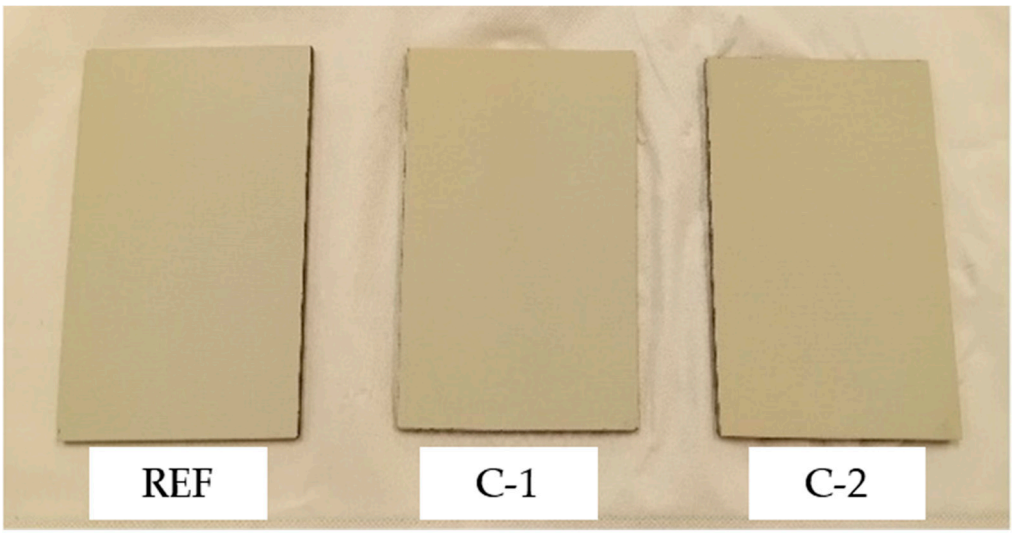

Figure 1. Different coatings used in this work: REF (reference AkzoNobel paint); C-1 and C-2 (superhydrophobic coatings by CIRA Company).

2.2. Methods

2.2.1. Hardness Test

Hardness tests were performed to compare the resistance to deformation of the REF, C-1, and C-2 coatings. The measurements were carried out using a Manual Digital Hardness Tester from Gibitre Instruments (Bergamo, Italy), following the ASTM D2240 standard [29] in Shore D configuration. This method involves applying a standardized force with a conical indenter to the coating surface, with hardness values directly measured from the device.

2.2.2. Thickness Measurements

The thickness of the REF, C-1, and C-2 coatings was measured using a PosiTector 6000 m from DeFelsko Inspection Instruments (Ogdensburg, NY, USA), which operates via magnetic induction. Since the composite substrate is not isotropic, the coatings were applied to a tinned steel sheet to ensure accurate measurements. The instrument detects thickness variations by measuring changes in the magnetic field between the probe and the metal substrate.

2.2.3. Roughness Measurements

Roughness measurements were performed by employing a SAMA SA6260 surface roughness meter according to the ISO 4288 [30]. The roughness measurements, reported as Ra, represent the arithmetic average of the absolute values of the profile height deviations from the mean line.

2.2.4. Contact Angle and Surface Free Energy (SFE) Measurements

Contact angle measurements were conducted to evaluate the wettability of the REF, C-1, and C-2 coatings on the composite substrate. A Dino-Lite digital microscope was used, and the tests followed ASTM D7490-13 [31]. Distilled water, formamide, and diiodomethane (all supplied by Merck-Sigma-Aldrich, Darmstadt, Germany) were used for the measurements [32].

Water contact angle measurements determined the degree of hydrophobicity, with surfaces classified as hydrophobic (contact angle > 90°) or hydrophilic (<90°). A superhydrophobic classification was assigned when the contact angle exceeded 150°.

The simplified Young model was employed to analyze and interpret the wetting behavior of the examined surfaces [33]. The Owens–Wendt model [34–36] was applied to calculate the SFE using the contact angles obtained with water, formamide, and diiodomethane [32]. The surface energy of the reference liquids used were 57 mJ/m^2 for formamide, 50.8 mJ/m^2 for diiodomethane, and 72.8 mJ/m^2 for water. The total surface energy was obtained by summing the polar and dispersive components.

2.2.5. Optical Microscopy

A Dino-Lite digital microscope was used to analyze and compare the surface morphology of the coatings. Observations were conducted at magnifications of 80× and 140×.

2.2.6. Scanning Electron Microscopy (SEM)

Morphological analysis at high magnifications was performed using a Carl Zeiss Auriga40 SEM (Oberkochen, Germany). The analysis was conducted under low vacuum without metallization, with magnifications ranging from 500× to 10,000×.

2.2.7. Ice Adhesion Test

The ice adhesion test was designed based on the methodology described in [26]. Since no standardized procedure exists for this type of test, a custom setup was developed to ensure reliable and repeatable measurements.

The test was carried out using an Ametek LR50KPlus mechanical testing machine from Lloyd Instruments (Bognor Regis, UK), as shown in Figure 2.

To create ice samples for adhesion testing, hollow cylindrical containers were 3D-printed using a BQ Hephestos 2 printer (Madrid, Spain) with Polylactic Acid (PLA, NatureWorks LLC, Blair, NE, USA), a material known for its ease of printing. Depending on laboratory availability, PLA in either blue or green was used. However, the color variation did not affect the composition or properties of the PLA. These PLA cylinders, with an internal diameter of 20 mm, an external diameter of 22 mm, and a height of 15 mm, acted as molds for water.

Initially, the composite samples 100 × 60 mm × mm with the REF, C-1, and C-2 coatings were placed on top of the PLA cylinders and stored in a freezer at −29 °C to allow the ice to form and adhere to the coatings. However, challenges arose with this setup, leading to the development of a custom 3D-printed base designed to securely hold both the composite sample and the water-filled cylinder. This base, visible in Figure 3 (top), featured:

- Two cylindrical housings to prevent movement of the cylinders;
- Two perpendicular sides at one corner to ensure correct alignment;
- Four support pillars to hold the composite sample above the cylinders.

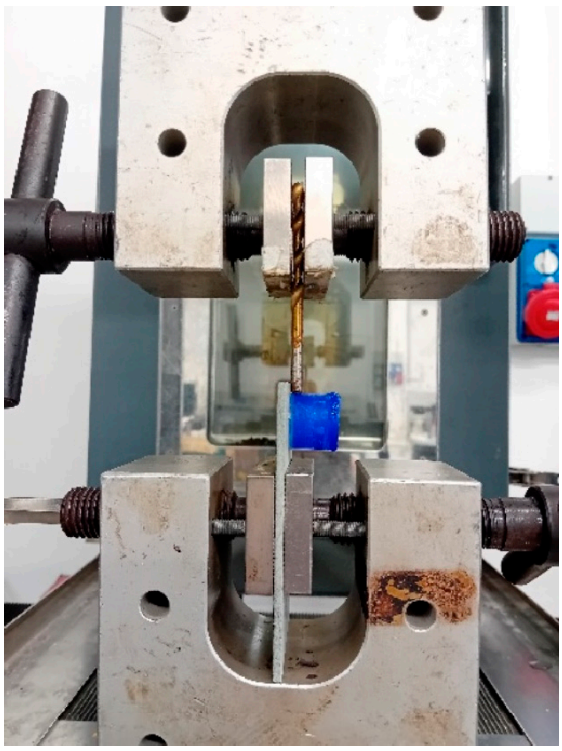

Figure 2. Setup of the ice adhesion strength.

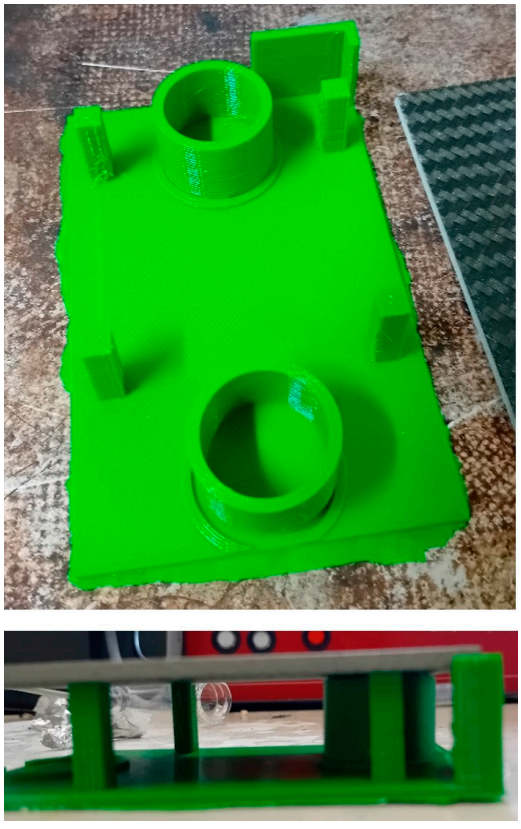

Figure 3. PLA base with two cylinders (**top**); composite sample placed on the base during the ice formation process (**bottom**).

The four pillars were designed to be 0.4 mm higher than the water-filled cylinders, allowing space for ice expansion during freezing. However, this gap was partially occupied by the convex meniscus formed between the water and the PLA container, ensuring contact between the water and the composite surface. As freezing progressed, the ice expanded into the available space, creating a bonded ice area of 100π mm^2, corresponding to the internal diameter of the PLA cylinder. A representation of the composite sample in contact with the water-filled cylinder is also shown in Figure 3 (bottom).

Once the water had fully frozen at −29 °C, adhering to the coated composite sample, the setup was transferred to the mechanical testing machine. The sample was clamped in a vertical position (Figure 2), and a force was applied to the ice using a cylindrical probe (5 mm in diameter) at a constant displacement rate of 1 mm/min. The probe was positioned close to the coated surface without touching it, ensuring that the ice was subjected exclusively to shear stress (τ). The adhesion strength was then calculated using Equation (1):

$$\tau = \frac{F}{A} \quad (1)$$

where F is the force applied by the testing machine and A is the bonded ice area (100 π mm^2). This approach allowed for a precise evaluation of the ice adhesion strength of the different coatings under controlled conditions.

3. Results

The results obtained from the different tests carried out on the coatings under analysis are presented below.

3.1. Characterization of Coatings

The results of the Shore D hardness test performed on the REF, C-1, and C-2 coatings are shown in Table 1.

Table 1. Results of Shore D hardness test performed on REF, C-1, and C-2 coatings.

Shore D Hardness		
REF	**C-1**	**C-2**
21.8 ± 1.0	23.4 ± 1.0	23.3 ± 1.1

A similar hardness value has been measured on both experimental coatings, equal to about 23, although C-1 and C-2 coatings have different compositions. It is important to underline that this value is higher (by about 7%) than the hardness measured on the reference coating, i.e., REF.

The mean thickness values, with the related confidence intervals, measured on the REF, C-1, and C-2 coatings are reported in Table 2.

Table 2. Results of thickness measurements carried out on REF, C-1, and C-2 coatings.

Thickness (μm)		
REF	**C-1**	**C-2**
33 ± 5	62 ± 6	59 ± 7

The thickness of the two coatings is similar. Furthermore, the low variation in results indicates that the spray application of the coatings was conducted uniformly, since, as expected, a lower value was observed for C-2.

The results of the roughness measurements, performed on coatings applied on metal plates and on composite substrates, are summarized in Table 3.

Table 3. Results of roughness measurements carried out on the coatings under analysis applied on metal plates or on a composite substrate.

Roughness (μm)					
REF		**C-1**		**C-2**	
Metal	Composite	Metal	Composite	Metal	Composite
3.0 ± 0.2	3.6 ± 0.4	6.4 ± 0.5	6.0 ± 1.2	6.2 ± 0.2	7.3 ± 1.7

As expected, both experimental coatings, i.e., C-1 and C-2, show higher roughness than the AkzoNobel reference. The high surface roughness plays a crucial role in incorporating and maintaining icephobic performance and is intrinsically interlinked with other surface-induced icephobicity strategies, including superhydrophobicity [37]. In the present study, the roughness of the C-1 and C-2 coatings was found to be higher than that reported for comparable systems in the literature. For instance, superhydrophobic silicone rubber surfaces prepared via micro compression molding exhibit Ra = 2.54 μm (μCM), while coatings treated with atmospheric pressure plasma (APP) display a significantly lower roughness of Ra = 0.70 μm [38]. Lotus leaf-inspired superhydrophobic surfaces with micro-/nano-scale surface textures reported by Ma et al. [39] showed an even lower Ra value of 0.562 μm. Additionally, other advanced coatings developed via chemical techniques—such as sol–gel processes, polyester-based formulations with fluorinated additives applied by electrostatic spray deposition, and silicone-based paints modified with alumina nanoparticles—demonstrate roughness values ranging from 0.19 to 2.84 μm [40].

The roughness values of the two experimental coatings are similar when applied to a metal plate; on the other hand, when applied to the composite, the roughness of the C-2 slightly exceeds that of the C-1.

The results of contact angle (CA) measurements, performed with water (H_2O), diiodomethane (CH_2I_2), or formamide ($HCONH_2$), are reported in Table 4. Images captured during the contact angle test performed on the different coatings using water are shown in Figure 4.

Table 4. Results of contact angle measurements performed on the three coatings using Water (W), Diodomethane (D), and Formamide (F) liquids.

Contact Angle (°)								
REF			**C-1**			**C-2**		
W	D	F	W	D	F	W	D	F
66.2 ± 7.7	48.4 ± 5.8	70.5 ± 3.1	154.3 ± 1.6	150.6 ± 4.7	154.0 ± 3.4	160.8 ± 4.3	149.4 ± 4.9	159.8 ± 2.2

The low wettability of the surface was also demonstrated by the behavior of 5 μL water droplets deposited onto the C-1 coated substrate inclined at an angle of 5°. Upon impact, the droplet promptly bounced off and then rolled off the surface, indicating minimal adhesion and confirming the water-repellent character of the coating (Figure 5). A similar behavior was observed for C-2; however, the corresponding results are not shown here for the sake of brevity. Conversely, in the case of the REF surface, the water droplet did not roll off but remained attached upon impact, indicating high surface adhesion.

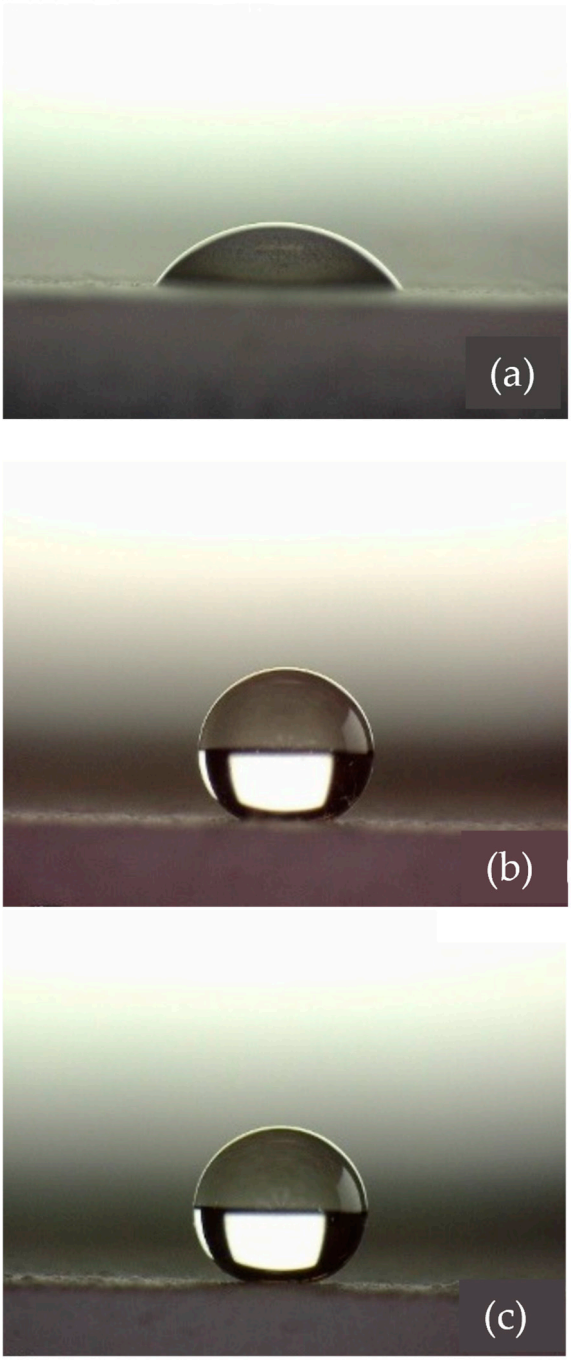

Figure 4. Image of the water droplet placed on the surface of REF (**a**), C-1 (**b**), and C-2 (**c**) coatings during contact angle tests.

Contact angle measurements using distilled water were used to determine the hydrophobic or hydrophilic nature of the coatings. According to the results reported in Table 4, and as can be observed in Figure 4a, the AkzoNobel reference paint is quite hydrophilic, as its average contact angle with water is less than 90°. On the other hand, C-1 and C-2 can both be classified as superhydrophobic coatings since their average contact angle is greater than 150° and 160°, respectively.

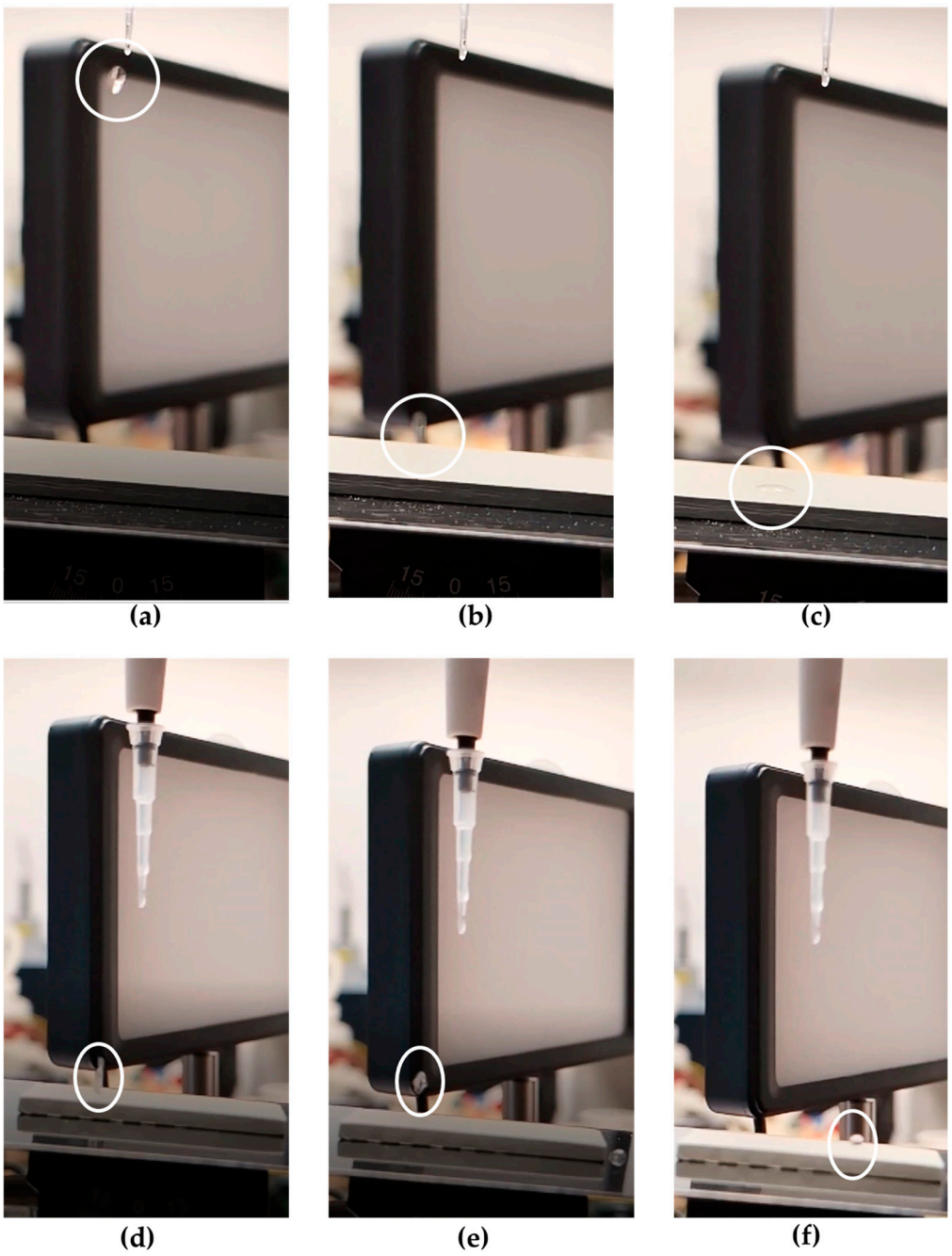

Figure 5. Images of the water droplet (highlighted with a white circle) falling down (**a**), approaching (**b**), and impacting (**c**) the REF surface, and impacting (**d**), bouncing off (**e**), and rolling off (**f**) the C-1 surface.

As already explained, the measurements performed with the other two liquids, i.e., Diiodomethane and Formamide, were used to calculate the SFE on each coating, according to the relationship reported by Owens [34–36]. The SFE of each coating, reported in Table 5, was calculated from the contact angle data reported in Table 4 using a Matlab-based solver developed at CIRA for this purpose [32]. Starting from the measured contact angles, the developed Matlab-based solver is designed to numerically solve the system of equations required to obtain optimized contact angle and solid's SFE.

Table 5. Surface free energy (SFE) calculated for each coating.

SFE (mJ/m^2)		
REF	**C-1**	**C-2**
38.7	0.36	0.24

As expected, the SFEs of the C-1 and C-2 coatings are much lower than that measured on the reference paint, i.e., AkzoNobel. The obtained values of SFE for C-1 and C-2 are significantly lower than those reported even for PTFE-based coatings [41]. Specifically, PTFE coatings on rough substrates (Ra = 4.50 μm) exhibit SFE values ranging between 19.52 and 23.46 mJ/m^2.

The optical microscope was used to analyze the surface of the different coatings at a medium magnification. The images reported in Figure 6 illustrate the surfaces of REF, C-1, and C-2 samples at 140× magnification.

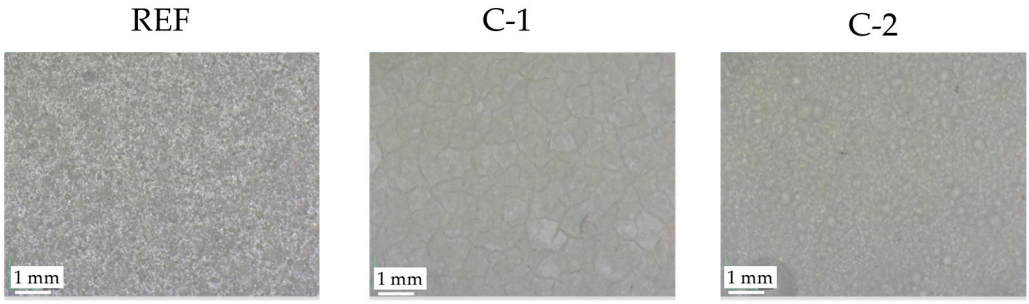

Figure 6. Microscopic observations of REF, C-1, and C-2 surfaces at 140×.

An examination of the previous images reveals that the C-1 surface presents plaques and cracks on its surface, while the C-2 sample shows spherical aggregations. Furthermore, in some areas of the C-2 sample, the microscope appears out of focus, confirming that C-2 has a high surface roughness, greater than C-1, as already highlighted by some roughness test results. This observation is supported by the absence of out-of-focus areas in the images of the C-1 coating, despite the fact that surface cracks can be seen on it.

In order to obtain an examination of the surface of the three coatings at higher magnifications, a scanning electron microscope (SEM) was employed. The SEM images taken on the surfaces of REF, C-1, and C-2 coatings at different magnifications are shown in Figure 7.

SEM images of the REF sample (i.e., the AkzoNobel paint) reveal a relatively smooth surface, with the coating applied uniformly. This observation is in line with the results of the roughness measurements, with low values observed for the REF coating compared to the others. Interestingly, the structures of the superhydrophobic coatings do not show the typical two-length scale hierarchical structure which is usually observed in superhydrophobic surfaces [42,43]. This important finding highlights that, regardless of the specific morphological features or roughness patterns generated on the surface, the combination of surface texturing with appropriate chemical modification, capable of significantly lowering the SFE, is sufficient to achieve superhydrophobicity.

Some thin cracks appear on the surface of the C-1 coating. However, they do not appear to influence the contact angle values measured on this coating, as previously presented, and hence the superhydrophobic character of this coating. This finding is in agreement with the results reported by Aslanidou et al. [44], according to which grooves formed during the preparation of superhydrophobic coatings did not significantly impact the contact angles of water and glycerol drops, which remained high.

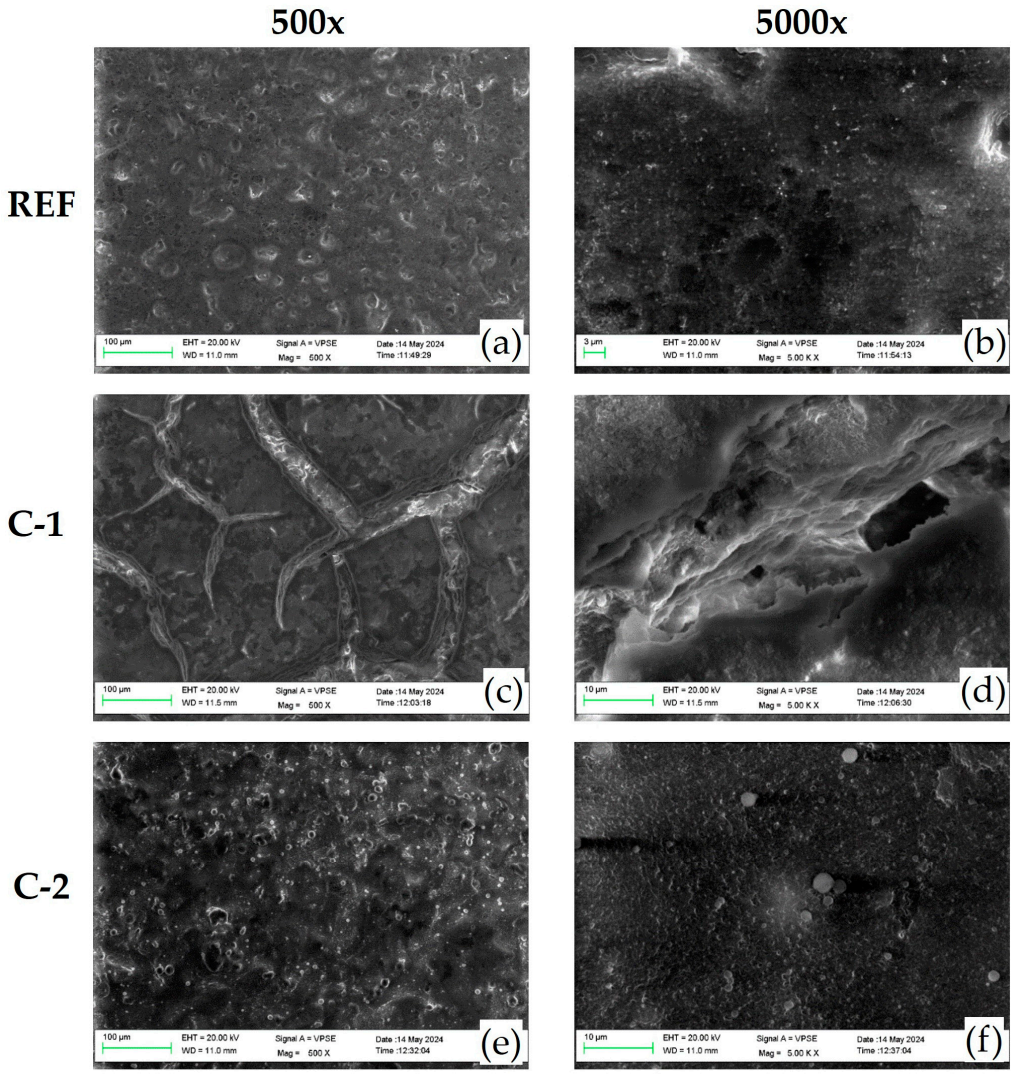

Figure 7. SEM images of REF at 500× (**a**) and 5000× (**b**), C-1 at 500× (**c**) and 5000× (**d**), and C-2 surfaces at 500× (**e**) and 5000× (**f**), respectively.

Finally, no fractures are detected on the surface of the C-2 coating; its surface appears uniform and similar to that of the AkzoNobel reference but with some spherical particles.

3.2. Ice Adhesion Results

Ice adhesion tests were performed following the original procedure described in Section 2.2.7.

Before performing the test, the samples were kept at a constant temperature of −29 °C. Considering t = 0 s as the time in which the sample was removed from the freezer, ice detachment (in test with a constant crosshead speed of 1 mm/min) occurred for all samples at t < 45 s. The environmental conditions in which the ice adhesion test was carried out (in the laboratory) were about 20 °C and 60% relative humidity. It was verified that during a time less than 45 s in the mentioned laboratory conditions, no substantial reduction in the contact area between ice and the surface of each coating occurred. However, of the numerous tests carried out in particular for C-1 and C-2 coatings, some of them were not reliable, probably due to the intrinsic superhydrophobic nature of the two coatings which, therefore, made it difficult for ice to adhere. The related results were therefore discarded.

Table 6 presents the average (valid) values of the stress of adhesion between each coating and ice. The ice/coating contact area used to calculate τ was assumed to be

constant and equal to 100π mm^2. In all cases, a non-negligible range of variation in results was observed.

Table 6. Average stress of adhesion between each coating and ice.

Average Adhesion Strength (kPa)		
REF	**C-1**	**C-2**
481.6 ± 136.3	48.5 ± 15.6	65.6 ± 11.5

From the observation of the data in Table 6, it is evident that both experimental coatings are capable of substantially reducing the adhesive resistance of the ice on the surface—by 90% for C-1 and 86% for C-2—and these results are in line with our expectations.

Figure 8 shows curves of breaking load vs. test time recorded during the ice adhesion test performed on each coating. From the observation of these graphs, the excellent behavior of the two experimental coatings is even more evident, which allows us to reduce the adhesion of the ice compared to the paint AkzoNobel. It is also evident that the time required for ice to detach from the coating surface during the test is much shorter for C-1 and C-2 than for the reference coating.

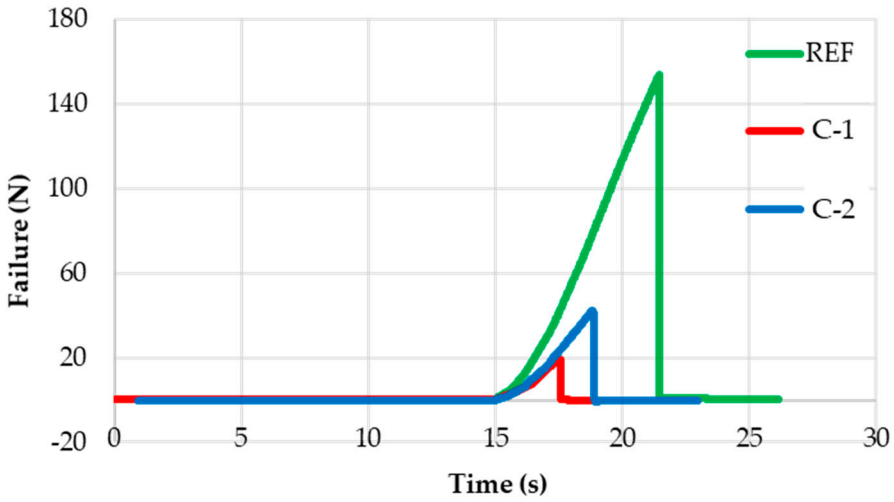

Figure 8. Ice adhesion test curves, in terms of breaking load versus time, for the REF, C-1, and C-2 coatings.

These results, in accordance with the low wettability exhibited by these coatings at low temperatures [45], are compliant with those measured by Rønneberg et al. [26] in the same setup configuration at −18 °C, a temperature close to the −29 °C used in the present work. For Al, they measured an Ice Adhesion Strength (IAS) of 393 ± 124 kPa, comparable with those measured in the present work. Differences must be ascribed to the different temperature of icing and mostly to the different nature of reference, being Aluminium 6061-T6 in [26] and AkzoNobel on the composite sheet in the present work. It is worth noting the comparisons between the IAS measurements performed on the commercial EC-3100, two-component, water-based, icephobic, non-stick coating from Ecological Coating, LLC (New York, NY, USA) [26,46] and the coated surfaces object in the present paper. In both cases, a substantial reduction in IAS values is observed compared to the related references, but the C-1 and C-2 provide values of IAS of 48.5 ± 15.6 kPa and 65.6 ± 11.5 kPa, which are considerably lower, i.e., −64% and −51%, respectively, than 135 ± 38 kPa measured for EC-3100. This result is unexpected, considering that the coatings developed in this work have a considerable roughness, i.e., 6.0 ± 1.2 µm for C-1 and 7.3 ± 1.7 µm for C-2,

while the commercial EC-3100 reference coating is smooth, as described in the technical datasheet [46]. Conversely, the time in which the detachment occurs seems to be slightly increased, namely about 17 and 18 s with respect to the 12–15 s measured in [26].

Rather, the IAS values exhibited by the rough C-1 and C-2 coatings appear to be more comparable to those reported for the same commercial smooth coating EC-3100, which was tested always at –18 °C, but using a centrifugal method, yielding values of 78 kPa ± 14 and 85 kPa ± 49. The two values refer to the same test performed in two different laboratories [26]. Compared to values measured with the centrifugal test, C-1 shows a reduction in IAS of −38% and −16% and C-2 of −43% and −23%.

In contrast, Shen et al. [47,48] reported a shear IAS of approximately 80 kPa on a superhydrophobic surface containing a hierarchical structure formed by sand-blasted microstructures and hydrothermally grown TiO_2 nanowires. Relative to this coating, C-1 and C-2 demonstrate IAS reductions of 39% and 18%, respectively.

Similarly, Du et al. [49], measured a horizontal shear IAS of 105.92 kPa and 177.36 kPa on TiO_2/polyurea superhydrophobic coating at −20 °C, again significantly higher than those recorded for C-1 and C-2.

Conversely, considerably lower IAS values were reported for PDMS-based coatings. For instance, Xie et al. [50] measured IAS values of 18.5 kPa and 8.5 kPa for certain interpenetrating epoxy/PDMS gel coatings. Likewise, Cheng et al. [51] reported an IAS of 6.5 kPa for PDMS/SiO2 based surfaces tested at −25.0 °C and high humidity conditions (60%).

4. Discussion and Conclusions

According to the definition reported in [52], the coatings developed in this work belong to the category of textured surfaces. They have been designed to increase the roughness of the reference surfaces, and the goal was achieved since the Ra increased by 67% and 103% in C-1 and C-2, respectively. Additionally, the hardness increased by 7% for both coatings when compared to the commercial aerospace coating used as a reference. The surface chemistry of reference was changed in order to drastically reduce the SFE by 99% in both coatings. As a consequence of both the morphological and chemical effect, the WCA of coated surfaces increased by 133 and 143% for C-1 and C-2. Indeed, as reported, the intrinsic superhydrophobic nature of the two coatings made it difficult for ice to adhere during the ice adhesion test. Nevertheless, the higher the roughness and the lower the SFE, the higher the WCA was for C-2 compared to C-1.

However, the increased roughness, while positively contributing to superhydrophobicity at room temperature, becomes a disadvantage at low temperatures. This is because, for the rougher coating C-2, a higher ice adhesion strength is observed compared to the less rough, superhydrophobic surface of C-1. Nevertheless, both surfaces, C-1 and C-2, improved ice detachment. In fact, the ice adhesion strength was reduced by 90% and 86% for C-1 and C-2, respectively, compared to the reference. This also means that the Cassie–Baxter effect is retained at really low temperature, i.e., −29 °C, and with ice attached to the surface in static conditions. Values are in line with those reported in Figure 3(bottom) of [52], which summarize the IAS of different icephobic surfaces from 162 journal papers. The ice formed statically on a surface is the most damaging, as it can lead to the deterioration of the surface morphology of superhydrophobic coatings if repeatedly detached [52].

The investigation of coating behavior under realistic outdoor conditions is crucial for assessing their practical applicability, especially in demanding operational environments. Aware of the importance of this aspect, specific tests are planned to be carried out in the near future. Previous tests simulating real flight conditions, including variations in temperature, altitude, and humidity conducted on similar formulations have demonstrated that the wettability of the coatings remains stable under such conditions [53]. Furthermore,

immersion tests in alkaline solutions, i.e., NaCl and NaOH, have also confirmed the chemical robustness of these kind of coatings, with no significant changes in wettability observed [54].

Aware of this, future work will be focused on the constant improvement of the coatings' effectiveness and durability in order to make this technology a real application as a passive IPS in combination with active systems. Furthermore, continuous effort will be addressed to improve the setup for the ice adhesion measurement, aiming to make uniform and comparable performed measurements, going towards a standardized method.

5. Patents

Data reported in this manuscript refer to coatings whose formulation is protected by the Italian Patent N. IT102021000032444, "Rivestimento superidrofobico e ghiacciofobico di un substrato, metodo per il suo ottenimento e substrato così rivestito", F. Piscitelli, 23 December 2021, and by the International Patent Application N° PCT/IB2022/062672 2022, "Substrate superhydrophobic and icephobic coating, method for obtaining it and substrate thus coated", F. Piscitelli, 22 December 2022.

Author Contributions: Conceptualization, F.P.; Data curation, F.P. and M.F. (Mariaenrica Frigione); Formal analysis, F.P.; Investigation, F.P., M.F. (Matteo Fanciullo), A.S. and M.C.; Methodology, F.P., A.S. and M.F. (Mariaenrica Frigione); Supervision, F.P.; Validation, F.P. and M.F. (Mariaenrica Frigione); Writing—original draft, F.P., M.F. (Matteo Fanciullo), A.S. and M.F. (Mariaenrica Frigione); Writing—review and editing, F.P. All authors have read and agreed to the published version of the manuscript.

Funding: This research was funded by The Italian Ministry for University and Research (MUR) through the National Aerospace Research Program (PRORA) D.I. n° 662/2020 as TECH-ICE project.

Institutional Review Board Statement: Not applicable.

Informed Consent Statement: Not applicable.

Data Availability Statement: The original contributions presented in this study are included in the article. Further inquiries can be directed to the corresponding author.

Acknowledgments: The authors gratefully acknowledge F. Montagna and G. Bruno for their technical support in the development of the setup for the ice adhesion tests.

Conflicts of Interest: The authors declare no conflicts of interest.

Abbreviations

The following abbreviations are used in this manuscript:

CIRA	Italian Aerospace Research Centre
IPS	Ice protection system
SFE	Surface Free Energy
IAS	Ice Adhesion Strength

References

1. Cao, Y.; Tan, W.; Wu, Z. Aircraft icing: An ongoing threat to aviation safety. *Aerosp. Sci. Technol.* **2018**, *75*, 353–385. [CrossRef]
2. Perkins, P.J.; Rieke, W.J. Aircraft icing problems—After 50 years. In Proceedings of the 31st Aerospace Sciences Meeting and Exhibit, Reno, NV, USA, 11–14 January 1993.
3. Potapczuk, M.G. Aircraft Icing Research at NASA Glenn Research Center. *J. Aerosp. Eng.* **2013**, *26*, 260–276. [CrossRef]
4. Bragg, M.B.; Broeren, A.P.; Blumenthal, L.A. Iced-airfoil aerodynamics. *Prog. Aerosp. Sci.* **2005**, *41*, 323–362. [CrossRef]
5. Thomas, S.K.; Cassoni, R.P.; MacArthur, C.D. Aircraft Anti-Icing and De-Icing Techniques and Modeling. *J. Aircr.* **1996**, *33*, 841–854. [CrossRef]
6. He, Q.; Li, K.; Xu, Z.; Wang, J.; Wang, X.; Li, A. Research Progress on Construction Strategy and Technical Evaluation of Aircraft Icing Accretion Protection System. *Chin. J. Aeronaut.* **2023**, *36*, 1–23. [CrossRef]

7. Piscitelli, F.; Ameduri, S.; Volponi, R.; Pellone, L.; De Nicola, F.; Albano, F.; Elia, G.; Notarnicola, L. Effect of Surface Modification on the Hybrid Ice Protection Systems Performances. In Proceedings of the International Conference on Icing of Aircraft, Engines, and Structures, Vienna, Austria, 20–22 June 2023; SAE Technical Paper 2023-01-1452. SAE International: Vienna, Austria, 2023. [CrossRef]
8. Maio, L.; Piscitelli, F.; Ameduri, S.; Concilio, A.; Ricci, F. Combining Ultrasound and Surface Treatments for an Efficient Ice Protection. In *European Workshop on Structural Health Monitoring*; EWSHM 2020. Lecture Notes in Civil Engineering; Rizzo, P., Milazzo, A., Eds.; Springer: Cham, Switzerland, 2021; Volume 127. [CrossRef]
9. Laforte, C.; Carriere, J.C.; Laforte, J.L. How a Solid Coating Can Reduce the Adhesion of Ice on a Structure. In Proceedings of the 10th International Workshop on Atmospheric Icing of Structures IWAIS, Brno, Czech Republic, 17–20 June 2002.
10. Golovin, K.; Kobaku, S.; Lee, D.; Di Loreto, E.; Mabry, J.; Tuteja, A. Designing durable icephobic surfaces. *Sci. Adv.* **2016**, *2*, e1501496. [CrossRef]
11. Andersson, L.O.; Golander, G.C.; Persson, S. Ice Adhesion to Rubber Material. *J. Adhes. Sci. Technol.* **1994**, *8*, 117–132. [CrossRef]
12. Boinovich, L.B.; Emelyanenko, A.M. Anti-Icing Potential of Superhydrophobic Coatings. *Mendeleev Commun.* **2013**, *23*, 3–10. [CrossRef]
13. Piscitelli, F.; Palazzo, S.; De Nicola, F. Icing Wind Tunnel Test Campaign on a Nacelle Lip-Skin to Assess the Effect of a Superhydrophobic Coating on Ice Accretion. *Appl. Sci.* **2023**, *13*, 5183. [CrossRef]
14. Farhadi, S.; Farzaneh, M.; Kulinich, S.A. Anti-icing performance of superhydrophobic surfaces. *Appl. Surf. Sci.* **2011**, *257*, 6264–6269. [CrossRef]
15. Saito, H.; Takai, K.; Yamauchi, G. Water- and ice-repellent coatings. *Surf. Coat. Int.* **1997**, *80*, 168–171. [CrossRef]
16. Piscitelli, F. Characterization in Relevant Icing Conditions of Two Superhydrophobic Coatings. *Appl. Sci.* **2022**, *12*, 3705. [CrossRef]
17. Borgaonkar, A.; McNamara, G. Environmental Impact and Life Cycle Cost Analysis of Superhydrophobic Coatings for Anti-Icing Applications. *Coatings* **2024**, *14*, 1305. [CrossRef]
18. Bleszynski, M.; Clark, E. Current Ice Adhesion Testing Methods and the Need for a Standard: A Concise Review. *Standards* **2021**, *1*, 117–133. [CrossRef]
19. McDonald, B.; Patel, P.; Zhao, B. Droplet freezing and ice adhesion strength measurement on super-cooled hydro-phobic surfaces. *J. Adhes.* **2017**, *93*, 375–388. [CrossRef]
20. Kulinich, S.; Farzaneh, M. Ice adhesion on super-hydrophobic surfaces. *Appl. Surf. Sci.* **2009**, *255*, 8153–8157. [CrossRef]
21. Saleema, N.; Farzaneh, M.; Paynter, R.W.; Sarkar, D.K. Prevention of ice accretion on aluminum surfaces by enhancing their hydrophobic properties. *J. Adhes. Sci. Technol.* **2011**, *25*, 27–40. [CrossRef]
22. Koivuluoto, H.; Stenroos, C.; Kylmälahti, M.; Apostol, M.; Kiilakoski, J.; Vuoristo, P. Anti-icing Behavior of Thermally Sprayed Polymer Coatings. *J. Therm. Spray Technol.* **2017**, *26*, 150–160. [CrossRef]
23. Arianpour, F.; Farzaneh, M.; Jafari, R. Hydrophobic and ice-phobic properties of self-assembled monolayers (SAMs) coatings on AA6061. *Prog. Org. Coat.* **2016**, *93*, 41–45. [CrossRef]
24. Kulinich, S.; Farzaneh, M. On ice-releasing properties of rough hydrophobic coatings. *Cold Reg. Sci. Technol.* **2011**, *65*, 60–64. [CrossRef]
25. Jafari, R.; Momen, G.; Farzaneh, M. Durability enhancement of icephobic fluoropolymer film. *J. Coat. Technol. Res.* **2016**, *13*, 405–412. [CrossRef]
26. Rønneberg, S.; Zhuo, Y.; Laforte, C.; He, J.; Zhang, Z. Interlaboratory Study of Ice Adhesion Using Different Techniques. *Coatings* **2019**, *9*, 678. [CrossRef]
27. Piscitelli, F. Rivestimento Superidrofobico e Ghiacciofobico di un Substrato, Metodo per il suo Ottenimento e Substrato Così Rivestito. Italian Patent N. IT102021000032444, 23 December 2021.
28. Piscitelli, F. Substrate Superhydrophobic and Icephobic Coating, Method for Obtaining It and Substrate Thus Coated. International Patent Application N° PCT/IB2022/062672, 22 December 2022.
29. *ASTM D2240-15*; Standard Test Method for Rubber Property—Durometer Hardness. ASTM International: West Conshohocken, PA, USA, 2015.
30. *ISO 4288*; Geometrical Product Specifications (GPS)–Surface Texture: Profile Method–Rules and Procedures for the Assessment of Surface Texture. International Organization for Standardization: Geneva, Switzerland, 1996.
31. *D7490-13*; Standard Test Method for Measurement of the Surface Tension of Solid Coatings, Substrates and Pigments Using Contact Angle Measurements. American Society for Testing and Materials: West Conshohocken, PA, USA, 2013.
32. Piscitelli, F.; Chiariello, A.; Dabkowski, D.; Corraro, G.; Marra, F.; Di Palma, L. Superhydrophobic Coatings as Anti-Icing Systems for Small Aircraft. *Aerospace* **2020**, *7*, 2. [CrossRef]
33. Young, T. An essay on the cohesion of fluids. *Philos. Trans. R. Soc. Lond.* **1805**, *95*, 65–87.
34. Owens, D.K.; Wendt, R.C. Estimation of the surface free energy of polymers. *Appl. Surf. Sci.* **1969**, *13*, 1741–1747. [CrossRef]
35. Żenkiewicz, M. Methods for the calculation of surface free energy of solids. *J. Achiev. Mater. Manuf. Eng.* **2007**, *24*, 137–145.

36. Rudawska, A.; Jacniacka, E. Analysis of Determining SFE Uncertainty with the Owens-Wendt method. *Int. J. Adhes. Adhes.* **2009**, *29*, 451–457. [CrossRef]
37. Memon, H.; Wang, J.; Hou, X. Interdependence of Surface Roughness on Icephobic Performance: A Review. *Materials* **2023**, *16*, 4607. [CrossRef]
38. Maghsoudi, K.; Vazirinasab, E.; Momen, G.; Jafari, R. Icephobicity and Durability Assessment of Superhydrophobic Surfaces: The Role of Surface Roughness and the Ice Adhesion Measurement Technique. *J. Mater. Process. Technol.* **2021**, *288*, 116883. [CrossRef]
39. Ma, L.; Wang, S.; Zhang, Z.; Liu, Y.; He, J.; Li, Y. Bio-Inspired Icephobic Coatings for Aircraft Icing Mitigation: A Critical Review. *Prog. Adhes. Adhes.* **2021**, *6*, 171–201.
40. Rivero, P.J.; Rodriguez, R.J.; Larumbe, S.; Monteserín, M.; Martín, F.; García, A.; Agüero, A. Evaluation of Functionalized Coatings for the Prevention of Ice Accretion by Using Icing Wind Tunnel Tests. *Coatings* **2020**, *10*, 636. [CrossRef]
41. Selvakumar, N.; Barshilia, H.C.; Rajam, K.S. Effect of Substrate Roughness on the Apparent Surface Free Energy of Sputter Deposited Superhydrophobic Polytetrafluoroethylene Coatings: A Comparison of Experimental Data with Different Theoretical Models. *J. Appl. Phys.* **2010**, *108*, 014910. [CrossRef]
42. Ebert, D.; Bhushan, B. Durable lotus-effect surfaces with hierarchical structure using micro- and nanosized hydrophobic silica particles. *J. Colloid Interface Sci.* **2012**, *368*, 584–591. [CrossRef]
43. Li, J.; Zhou, L.; Yang, N.; Gao, C.; Zheng, Y. Robust superhydrophobic coatings with micro- and nano-composite morphology. *RSC Adv.* **2017**, *7*, 44234–44238. [CrossRef]
44. Cui, M.; Shen, Y.; Tian, H.; Yang, Y.; Feng, H.; Li, J. Influence of Water Adhesion of Superhydrophobic Surfaces on Their Anti-Corrosive Behavior. *Surf. Coat. Technol.* **2018**, *347*, 38–45. [CrossRef]
45. Piscitelli, F. Superhydrophobic Coatings for Aeronautical Applications. In Proceedings of the 2020 IEEE International Workshop on Metrology for AeroSpace, MetroAeroSpace 2020-Proceedings, Pisa, Italy, 22–24 June 2020; pp. 282–287.
46. Ecological Coatings. Icephobic Coatings Anti-Ice. Available online: http://www.ecologicalcoatings.com/icephobic.html (accessed on 28 March 2025).
47. Shen, Y.; Tao, H.; Chen, S.; Zhu, L.; Wang, T.; Tao, J. Icephobic/anti-icing potential of superhydrophobic Ti6Al4V surfaces with hierarchical textures. *RSC Adv.* **2015**, *5*, 1666–1672. [CrossRef]
48. Shen, Y.; Wu, X.; Tao, J.; Zhu, C.; Lai, Y.; Chen, Z. Icephobic materials: Fundamentals, performance evaluation, and applications. *Prog. Mater. Sci.* **2019**, *103*, 509–557. [CrossRef]
49. Du, Y.; Hu, L.; Dong, L.; Du, S.; Xu, D. Experimental study on anti-icing of robust TiO_2/polyurea superhydrophobic coating. *Coatings* **2023**, *13*, 1162. [CrossRef]
50. Xie, Q.; Hao, T.; Wang, C.; Kang, Z.; Shi, Z.; Zhang, J. The Mechanical Mechanism and Influencing Factors of Ice Adhesion Strength on Ice-Phobic Coating. *J. Mar. Sci. Eng.* **2021**, *9*, 315. [CrossRef]
51. Cheng, H.; Yang, G.; Li, D.; Li, M.; Cao, Y.; Fu, Q.; Sun, Y. Ultralow icing adhesion of a superhydrophobic coating based on the synergistic effect of soft and stiff particles. *Langmuir* **2021**, *37*, 12016–12026. [CrossRef]
52. He, Z.; Zhuo, Y.; Zhang, Z.; He, J. Design of Icephobic Surfaces by Lowering Ice Adhesion Strength: A Mini Review. *Coatings* **2021**, *11*, 1343. [CrossRef]
53. Piscitelli, F.; Tescione, F.; Mazzola, L.; Bruno, G.; Lavorgna, M. On a simplified method to produce hydrophobic coatings for aeronautical applications. *Appl. Surf. Sci.* **2019**, *472*, 71–81. [CrossRef]
54. Piscitelli, F.; Volpe, A. Superhydrophobic Coatings for Corrosion Protection of Stainless Steel. *Aerospace* **2024**, *11*, 3. [CrossRef]

Disclaimer/Publisher's Note: The statements, opinions and data contained in all publications are solely those of the individual author(s) and contributor(s) and not of MDPI and/or the editor(s). MDPI and/or the editor(s) disclaim responsibility for any injury to people or property resulting from any ideas, methods, instructions or products referred to in the content.